# Photoionization Cross-Sections for the trans-iron element $Se^+$ from 18 eV to 31 eV

**B M McLaughlin[1,2]† and C P Ballance[3]‡**

[1]Centre for Theoretical Atomic, Molecular and Optical Physics, School of Mathematics and Physics, The David Bates Building, 7 College Park, Queen's University Belfast, Belfast BT7 1NN, UK
[2]Institute for Theoretical Atomic and Molecular Physics, Harvard Smithsonian Center for Astrophysics, Cambridge, MA 02138, USA
[3]Department of Physics, 206 Allison Laboratory, Auburn University, Auburn, AL 36849, USA

**Abstract.** Absolute photoionization cross-section calculations are presented for $Se^+$ using large-scale close-coupling calculations within the Breit-Pauli and Dirac-Coulomb R-matrix approximations. The results from our theoretical work are compared with recent measurements [1, 2, 3] made at the Advanced Light Source (ALS) radiation facility in Berkeley, California, USA. We report on results for the photon energy range 18.0 eV – 31.0 eV, which spans the ionization thresholds of the $^4S^o_{3/2}$ ground state and the low-lying $^2D^o_{5/2,3/2}$ and $^2P^o_{3/2,1/2}$ metastable states. Metastable fractions are inferred from our present work. Resonance energies and quantum defects of the prominent Rydberg resonances series identified in the spectra are compared for the 4p $\rightarrow$ nd transitions with the recent ALS experimental measurements made on this complex trans-iron element.

(Figures are in colour only in the online version)

PACS numbers: 32.80.Dz, 32.80.Fb, 33.60-q, 33.60.Fy

Short title: Photoionization of $Se^+$ ions

J. Phys. B: At. Mol. Opt. Phys: 27 February 2013

† Corresponding author, E-mail: b.mclaughlin@qub.ac.uk
‡ Corresponding author, E-mail: ballance@physics.auburn.edu

## 1. Introduction

Recently, detailed photoionization cross-section measurements for the trans-iron element $Se^+$, carried out at the Advanced Light Source (ALS) synchrotron radiation facility in Berkeley, California were reported in the literature [1, 2, 3]. The photon energy studied in the experiments ranged from 18.0 eV to 31.0 eV and was scanned with a nominal spectral resolution of 28 meV. Measurements were also made at a higher photon energy resolution of 5.5 meV from 17.75 to 21.85 eV spanning the $4s^24p^3\ {}^4S^o_{3/2}$ ground-state ionization threshold and the ${}^2P^o_3/2$, ${}^2P^o_{1/2}$, ${}^2D^o_{5/2}$, and ${}^2D^o_{3/2}$ metastable state thresholds. Although detailed resonance structure in the photoionization spectra was reported, it was not possible to positively determine the metastable components in the ion beam. Photoionization cross section calculations have been made recently on this complex ion using AUTOSTRUCTURE [4] within the Multi-Configuration-Breit-Pauli (MCBP) distorted-wave approximation for a wider range of energies and for higher charged states. It was concluded from that study on Se ions [4] (by visual comparison) that best agreement with experiment was obtained by weighting the contribution of the ground configuration states (${}^4S^o_{3/2}$, ${}^2D^o_{3/2}$, ${}^2D^o_{5/2}$, ${}^2P^o_{1/2}$, ${}^2P^o_{3/2}$) by (0.53, 0.15, 0.05, 0.11, 0.16) respectively. As pointed out by Sterling and Witthoeft [4], R matrix techniques are necessary to reproduce resonance interference effects. In the present work we report on large scale photoionization cross section calculations for this complex trans-iron ion in both the Breit-Pauli and Dirac Coulomb R-matrix approximations. We infer metastable fractions and benchmark our theoretical results with the available experimental data [1, 2, 3] providing confidence in the data on this trans-iron element for applications [5, 6].

Photoionization (PI) of atomic ions is an important process in determining the ionization balance and hence the abundances of elements in photoionized astrophysical nebulae. It has recently become possible to detect neutron($n$)-capture elements (atomic number $Z > 30$, e.g. Se, Kr, Br, Xe, Rb, Ba and Pb) in a large number of ionized nebulae [7, 8, 9]. These elements are produced by slow or rapid $n$-capture nucleosynthesis (the "$s$-process" and "$r$-process," respectively) [8, 10]. Measuring the abundances of these elements helps to reveal their dominant production sites in the Universe, as well as details of stellar structure, mixing and nucleosynthesis [11, 12, 13, 14, 15, 16, 17, 5]. These astrophysical observations are the motivation to determine the photoionization and recombination properties of $n$-capture elements.

Various $n$-capture elements have been detected in the spectra of planetary nebulae (PNe§), the photoionized ejecta of evolved low- and intermediate-mass stars (1–8 solar masses). Planetary Nebula progenitor stars may experience $s$-process nucleosynthesis [14, 18], in which case their nebulae will exhibit enhanced abundances of trans-iron elements. The level of $s$-process enrichment for individual elements is strongly sensitive to the physical conditions in the stellar interior [14, 16].

The underlying difficulty in studying $s$-process enrichment in PNe is due to the large uncertainties (factors of 2–3) of $n$-capture element abundances derived from the observational data [2, 5]. There are two main causes for these uncertainties. First, the low cosmic abundances of trans-iron elements, means their emission lines are sufficiently weak that generally only one or two ions of each element can be detected in individual PNe. Second, while robust ionization corrections can be derived

§ Following astrophysical nomenclature, we abbreviate the singular form planetary nebula as "PN" and the plural form as "PNe."

from numerical simulations of nebulae [19, 20], this method relies on the availability of accurate atomic data for processes that affect the ionization equilibrium of each element. In photoionized nebulae, these atomic data include photoionization cross-sections and rate coefficients for radiative and dielectronic recombination and charge exchange reactions are unknown for nearly all $n$-capture element ions. Uncertainties in the photoionization and recombination data of $n$-capture element ions can result in elemental abundance uncertainties of a factor of two or more [7].

The present theoretical investigation is a study to determine the photoionization and recombination properties of $n$-capture element ions, motivated by the astrophysical detection of these species and the importance of their elemental abundances for testing theories of nucleosynthesis and stellar structure. Determining the appropriate atomic data over the range of energies and temperatures encountered in astrophysical environs necessitates a predominantly theoretical approach. Experimental measurements are helpful to validate theoretical studies, particularly in the case of complex heavy ionic systems such as low charge states of trans-iron elements. We note that experimental studies are often limited in the photon energy range studied, energy resolution and to the charge states able to be investigated. In addition, many of the experiments carried out are contaminated by metastable states and require theoretical estimates to help unravel the components in the ion beam.

The prime motivation for choosing Se as the first element for investigation is due to the fact it has been detected in nearly twice as many PNe (70 in total) as any other trans-iron elements [9] in addition to recent experimental measurements becoming available to compare with [1, 2]. Experimental photoionization studies of other astrophysically observed $n$-capture elements have already been conducted by various groups in the cases of select Kr [21, 22, 23] and Xe ions [24, 23].

In this paper we present theoretical determinations of the absolute $Se^+$ photoionization cross-section near the ground-state ionization threshold and compare our results with recent experimental measurements [1, 2] for this trans-iron ion. We note that the results from our work can be applied to calibrate a broader theoretical effort to determine the photoionization and recombination properties of $n$-capture element ions over a large range of energies and temperatures. Our data would be suitable for incorporation within photoionization modelling codes such as Cloudy and XSTAR[19, 20], which numerically simulate the thermal and ionization structure of astrophysical nebulae. Photoionization models can be used to derive accurate and robust ionization corrections for trans-iron elements, thereby enabling the accurate determination of their abundances in the Universe. We also intend to explore the properties of other members of this iso-electronic sequence, for example, $Br^{2+}$ and $Rb^{3+}$ along with other low-charged Se ions in subsequent publications.

The layout of this paper is as follows. Section 2 presents a brief outline of the theoretical work. Section 3 presents our theoretical PI cross sections results where comparisons are made with the recent $Se^+$ photoionization experimental measurements [1, 2, 3]. Resonance energies and quantum defects for the various dominant Rydberg series (seen in both the experimental and theoretical photoionization spectra) are tabulated and compared. Finally in section 4 conclusions are drawn from the present investigation.

## 2. Theory

Relativistic corrections can play an increasingly significant role for atoms with charge $Z \geq 18$ [25]. It was shown in recent work on electron-impact excitation of neutral neon ($Z = 10$) that a $jK$ coupling scheme was required to accurately describe even the low lying energy target levels [26]. The semi-relativistic Breit-Pauli R-matrix approach has been successfully applied repeatably to atomic ions below Z=30 for numerous atomic systems by the Iron Project [27]. For atomic ions with $Z > 30$, a Dirac-Coulomb approach to electron and photon interactions is ideal, due to the importance of relativistic and correlation effects in accurately modelling these systems

Computationally, the increased number of relativistic orbitals over the corresponding non-relativistic orbitals can cause a dramatic increase both in the number of integrals required and in the complexity of the angular algebra. We note that in a recent work for the electron-impact excitation of $Fe^{4+}$ [28] and $Fe^{5+}$ [29] hundreds of millions of Racah coefficients were calculated for the relativistic treatment of this open-d shell system. To address the future challenge of electron scattering in which hundreds of levels and thousands of scattering channels are to be considered an efficient parallel version [30] of the DARC [31, 32, 33, 34] suite of codes was developed.

A natural extension of this work was the formation of the numerous bound-free dipole matrix elements required for photoionization in an equally efficient manner, distributed over an equivalent number of processors. This enables photoionization and photo-recombination calculations on complex halogen-like ions for example, $Ar^+$, $Kr^+$ and $Xe^+$, to be carried out at the same degree of accuracy [35] as those for electron impact excitation. It should be noted that in addition to large scale relativistic photoionization calculations, the same dipole matrix elements are the foundation of radiationally damped electron-impact excitation studies required in highly charged ions. With these extensions to the DARC codes one can address the complex problem of trans-iron element single photon ionization. The flowchart in figure 1, with brief annotations beside each module of the suite of DARC codes, illustrates the R-matrix sequence required to obtain photoionization cross sections with the parallel **D**irac **A**tomic **R**-matrix **C**odes. These recent modifications now include the concurrent formation of every dipole matrix, reducing the total time substantially required for the formation of all dipoles to that required by a single dipole. These developments open the frontier to enabling comprehensive pioneering large scale calculations along iso-nuclear sequences to be performed now within a feasible time frame.

Using this suite of DARC codes detailed photoionization cross section calculations for the $Se^+$ ion were performed for the ground and all the excited metastable levels associated with the $4s^24p^3$ configuration. To benchmark our theoretical results we compare them with recent high resolution experimental measurements made at the Advanced Light Source synchrotron radiation facility [1, 2, 3].

In R-matrix theory, all photoionization cross section calculations require the generation of atomic orbitals based primarily on the atomic structure of the residual ion. The present theoretical work for the photoionization of the $Se^+$ ion employs relativistic atomic orbitals generated for the residual $Se^{2+}$ ion, which were calculated using the extended-optimal-level (EOL) procedure within the GRASP structure code [36, 37, 25]. We explored various structure and scattering models of increasing complexity with the R-matrix approach in order to investigate an optimum model for determining the total photoionization cross sections.

Photoionization cross section calculations for this complex trans-iron system

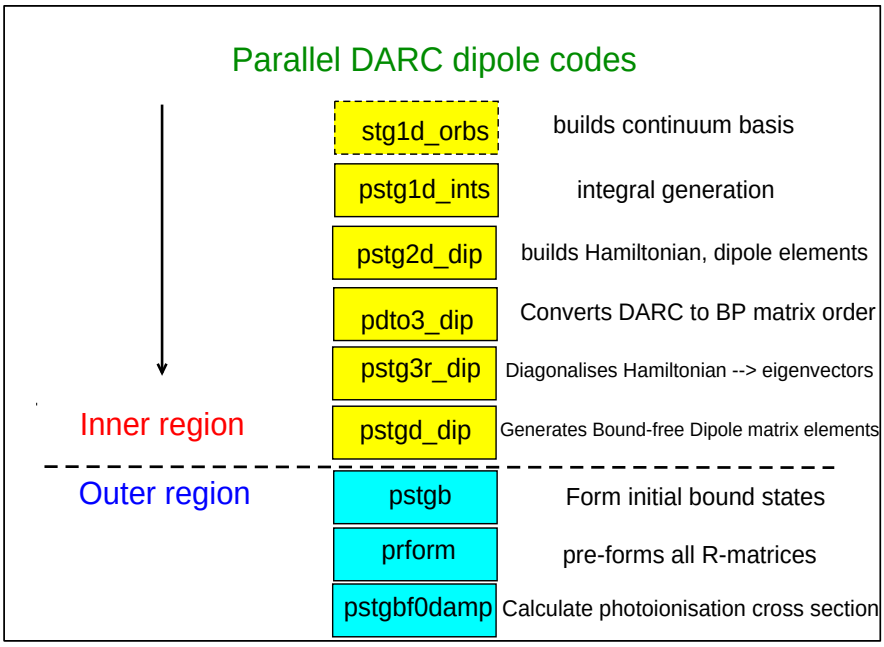


**Figure 1.** Flowchart illustrating the steps necessary to obtain photoionization cross sections with the parallel Dirac Atomic R-matrix Codes (DARC). The codes are available at http://connorb.freeshell.org/codes/DARCdipole/.

began by including only levels from the $4s^24p^2$, $4s4p^3$ and $4p^4$ configurations which gave rise to 20 $J\pi$ levels. We found this model to be inadequate to represent the complex experimental spectrum and it was necessary to extend the theoretical model. Our first approach was to supplement the configurations of this 20 level model with addition levels from several 3d-hole configurations, $3d^94s^24p^3$, $3d^94s4p^4$ and $3d^94p^5$. This increased the number of levels in our close coupling expansion to 126 yielding improved agreement with experiment. Further extensive theoretical models were then investigated with the inclusion of levels from configurations involving a 4d orbital in our close coupling expansion rather than levels from the 3d hole configurations. The first of these models included all 246 levels arising from the eight configurations: $4s^24p^2$, $4s4p^3$, $4p^4$, $4s^24p4d$, $4s^24d^2$, $4p^24d^2$, $4s4p^24d$ and $4p^34d$ were included in the close-coupling expansion. The second model investigated was when this 246-level model was augmented with levels from an additional $4s4p4d^2$ configuration, giving rise to a total of 336 levels.

The final model augmented this 336-level model with the $4s^24p5s$, $4s^24p5p$ and

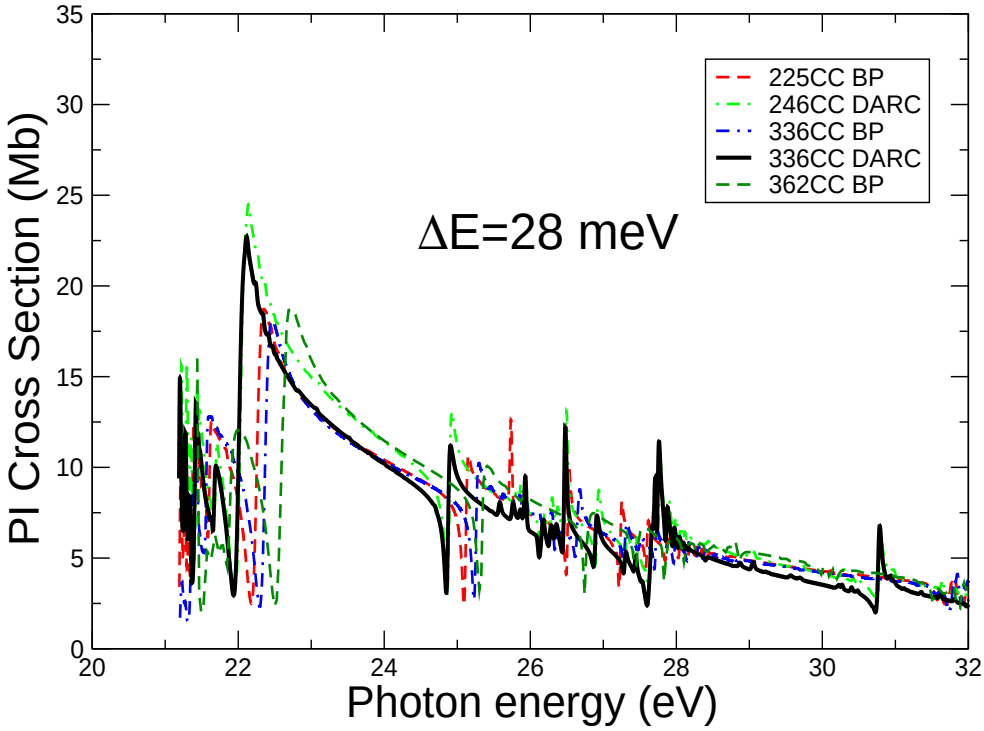


**Figure 2.** (Colour online) Photoionization of the $^4S^o_{3/2}$ ground state of the $Se^+$ ion. The cross section from threshold to a photon energy of 30 eV are illustrated. Theoretical results have been obtained from both the DARC and Breit-Pauli approximations with an increasing number of levels included in the close-coupling approximations. The theoretical cross sections have been convoluted with a 28 meV FWHM gaussian distribution for comparison purposes.

$4s^24p5d$ configurations which gave rise to a total of 362-levels. Table 1 shows a sample comparison of our results for the lowest 12 levels of the residual $Se^2$ (Se III) ion with the available experimental and theoretical work.

Photoionization cross section calculations were performed in the Dirac-Coulomb and Breit-Pauli approximation with the various models. The advantage of the DARC calculation over the Breit-Pauli result is marginal for the photoionization of outer shell electrons. However, it does provide the repeatability of the result using completely independent structure codes and for the most part independent collisional codes to provide the cross section.

Considering the ionization potential between the ground state of Se II and that of Se III is approximately 1.6 Ryds and according to NIST tables the $4s^24p4d$, $4s^24p5\ell$ levels are over 1 Ryd above the Se III ground state. This gives a photon energy of greater than 36 eV to photoexcite to either the $4d^24p4d$ or the $4s^24p5s$ levels.

**Table 1.** Comparison of the theoretical energies using GRASP and the Breit-Pauli approximation from the 362-level model with previous work, relative energies are in Rydbergs. A sample of the first 12 levels of the Se III ion are compared with AUTOSTRUCTURE [4] and the NIST [38] tabulated values.

| Level | Config. | Term[a] | Energy NIST | Energy GRASP | Energy Breit-Pauli[d] | Energy AUTOS[e] | $\Delta(\%)$[b] |
|---|---|---|---|---|---|---|---|
| 1 | $4s^24p^2$ | $^3P_0$ | 0.000000 | 0.000000 | 0.00000 | 0.00000 | 0.0 |
| 2 | $4s^24p^2$ | $^3P_1$ | 0.015870 | 0.015061 | 0.01419 | 0.01580 | 5.1 |
| 3 | $4s^24p^2$ | $^3P_2$ | 0.035880 | 0.035409 | 0.03347 | 0.03620 | 1.3 |
| 4 | $4s^24p^2$ | $^1D_2$ | 0.118760 | 0.140979 | 0.13835 | 0.14370 | 18.7 |
| 5 | $4s^24p^2$ | $^1S_0$ | 0.259070 | 0.285184 | 0.27116 | 0.25950 | 10.1 |
| 6 | $4s^14p^3$ | $^5S^o_2$ | 0.579910[c] | 0.566575 | 0.55304 | – | 2.3 |
| 7 | $4s^14p^3$ | $^3D^o_1$ | 0.830080 | 0.853381 | 0.81498 | 0.83080 | 2.8 |
| 8 | $4s^14p^3$ | $^3D^o_2$ | 0.844950 | 0.854258 | 0.81543 | 0.84500 | 1.1 |
| 9 | $4s^14p^3$ | $^3D^o_3$ | 0.879810 | 0.859092 | 0.81900 | 0.87980 | 2.3 |
| 10 | $4s^14p^3$ | $^3P^o_0$ | 0.970335 | 0.991048 | 0.94428 | 0.96750 | 2.1 |
| 11 | $4s^14p^3$ | $^3P^o_2$ | 0.970636 | 0.994054 | 0.94614 | 0.96540 | 2.4 |
| 12 | $4s^14p^3$ | $^3P^o_1$ | 0.971329 | 0.992406 | 0.94616 | 0.96760 | 2.2 |

[a] $^{2S+1}L^\pi_J$

[b] GRASP, absolute percentage difference relative to NIST values

[c] Esteves PhD thesis [1]

[d] Breit-Pauli

[e] Sterling and Witthoeft [4]

Therefore, their influence on the ground state photoionization cross section within the energy range presented in this paper, is solely in terms of changes in structure through CI mixing.

Figure 2 shows that the inclusion of the additional 5s, 5p and 5d orbitals in the basis set has a minimal effect on the total photoionization cross section for the $^4S^o_{3/2}$ ground state over the energy range investigated and for energies less than 31 eV. However, these comparisons with experiment are slightly misleading as the energy levels of the DARC R-matrix calculation are shifted to experimental values prior to the matrix diagonalization. Since converged results are obtained within the 336 level model we used this approximation to determine all the remaining PI cross sections for the metastable states with the DARC codes.

The R-matrix boundary radius of 8 Bohr radii was sufficient to envelop the radial extent of all the atomic orbitals of the residual $Se^{2+}$ ion. A basis of 16 continuum orbitals was sufficient to span the incident experimental photon energy range of up to 32 eV. The 336-state model produced a maximum of 1758 coupled channels in our scattering work with Hamiltonian matrices of dimension of the order of 28,300 by 28,300 in size. Due to dipole selection rules, for total ground state photoionization we need only consider the three bound-free dipole matrices, $2J^\pi = 3^o \rightarrow 2J^\pi = 1^e, 3^e, 5^e$ whereas for the excited metastable states one requires $2J^\pi = 5^o \rightarrow 2J^\pi = 3^e, 5^e, 7^e$ the $2J^\pi = 3^o \rightarrow 2J^\pi = 1^e, 3^e, 5^e$ and $2J^\pi = 1^o \rightarrow 2J^\pi = 1^e, 3^e$ bound-free dipole matrices. For each initial state the outer region electron-ion collision problem was solved (in the resonance region below and between all thresholds) using a suitably chosen fine

energy mesh of $5\times10^{-7}$ Rydbergs ($\approx$ 6.8 $\mu$eV) to fully resolve all the extremely fine resonance structure in the appropriate photoionization cross sections. The multi-channel R-matrix eigenphase derivative (QB) technique (applicable to atomic and molecular complexes) of Berrington and co-workers [39, 40, 41] was used to determine the resonance parameters. In the QB method, the resonance width $\Gamma$ is determined from the inverse of the energy derivative of the eigenphase sum $\delta$ at the position of the resonance energy $\epsilon_r$ via

$$\Gamma = 2\left[\frac{d\delta}{dE}\right]^{-1}_{E=\epsilon_r} = 2[\delta']^{-1}_{E=\epsilon_r} \quad . \tag{1}$$

Prominent photoexcitation-autoionization Rydberg resonances series are analyzed and identified as 4p $\rightarrow$ nd transitions, and the metastable fractions of the experimental $Se^+$ ion beam are estimated. Finally, in order to compare directly with recent experimental work on this system [1, 2, 3], the theoretical cross sections were convoluted with a gaussian function of appropriate width (FWHM of 28 meV and 5.5 meV respectively) and weighted accordingly in order to simulate the energy resolution of the measurements performed at the Advanced Light Source (ALS) synchrotron radiation facility.

## 3. Results and discussion

Figure 2 shows the convergence of the PI results obtained from the Breit-Pauli and Dirac-Coulomb (DARC) approximations for the $4s^24p^3\ {}^4S^o_{3/2}$ ground state using an n=4 basis. The theoretical PI cross section results are illustrated for the $4s^24p^3\ {}^4S^o_{3/2}$ ground state of this complex trans-iron element with an increasing number of levels retained in the close-coupling expansion. As illustrated in figure 2, the 336-state model yields a suitable description of these half collision processes for the $Se^+$ ion, where converged results are obtained with a larger close-coupling approximation. At this level of approximation it ensures consistency in our theoretical work. Using this 336-level model we obtained the PI cross sections for all the remaining metastable levels associated with the $4s^24p^3$ configuration within the Dirac-Coulomb (DARC) approximation. The theoretical PI cross section results for the individual levels arising from the $4s^24p^3$ configuration over the photon energy range 18 eV to 31 eV from the Dirac-Coulomb (DARC) approximation are shown in figure 3 where the results are convoluted with a gaussian distribution of 28 meV FWHM in order to compare with the high resolution ALS experimental results. The ALS measurements for $Se^+$ [2] were taken over the 18 eV to 31 eV photon energy range at an energy resolution of 28 meV, these measurements are illustrated in the bottom panel of figure 3. The absolute photoionization cross sections were measured at discrete photon energies and are shown in the figure by solid circles with their associated uncertainties.

To determine the fractions of metastable ions present in the experimental ion beam photoionization cross section calculations were performed using the Dirac-Coulomb R-matrix method for both the $^4S^o_{3/2}$ ground state and the excited metastable states ( $^2D^o_{3/2}$, $^2D^o_{5/2}$, $^2P^o_{1/2}$ and $^2P^o_{3/2}$ ) associated with the $4s^24p^3$ configuration. The individual fractions were estimated by first scaling the highest-lying metastable state to the absolute experimental cross section. Each subsequent state was then scaled such that the sum of the theoretical cross sections matched the experiment as closely as possible, with all four metastable states together with the ground state fractions

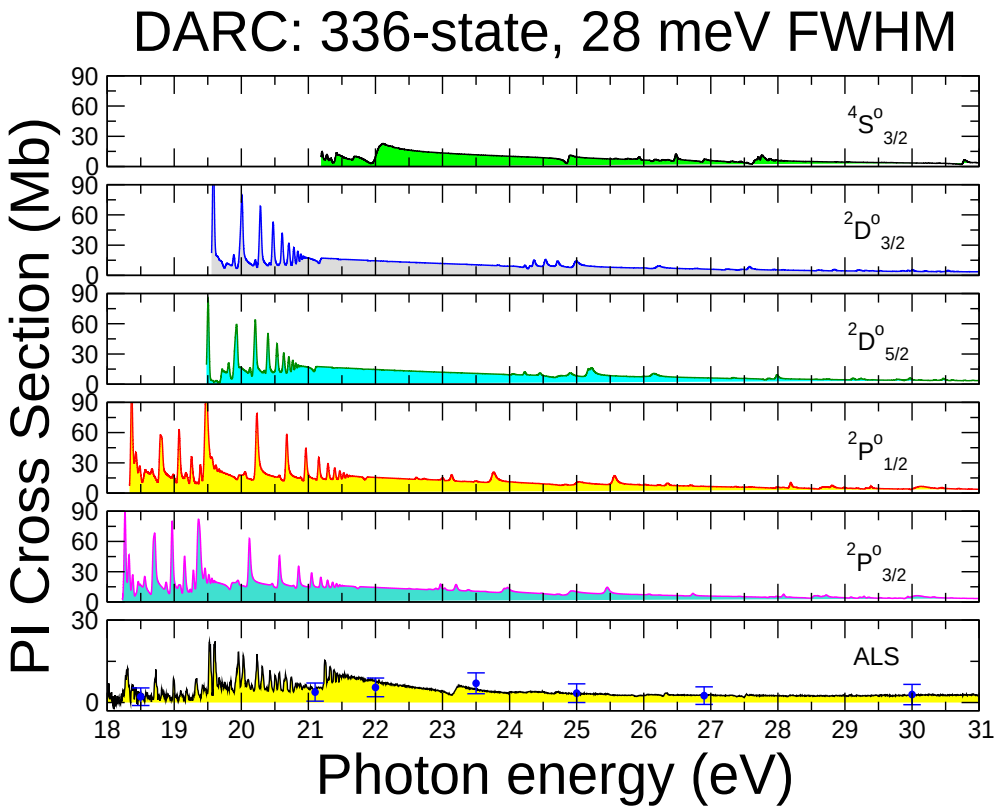


**Figure 3.** (Colour online) Theoretical photoionization cross sections (336-level close-coupling DARC calculations) for the $^4S^o_{3/2}$ ground state, $^2D^o_{3/2}$, $^2D^o_{5/2}$, $^2P^o_{3/2}$ and $^2P^o_{1/2}$ metastable states arising from the $4s^24p^3$ configuration are illustrated (Top 5 panels). The theoretical results were convoluted with a gaussian of 28 meV FWHM to simulate the photon energy resolution of the experimental measurements (bottom panel) taken at the Advanced Light Source synchrotron radiation facility.

ultimately constrained to sum to unity. Using this technique the various fractions were determined and it was found that a non-statistical distribution of the ground and metastable states gave best agreement with experiment by weighting the contribution of the $^4S^o_{3/2}$, $^2D^o_{3/2}$, $^2D^o_{5/2}$, $^2P^o_{1/2}$ and $^2P^o_{3/2}$ states by (0.52, 0.13, 0.19, 0.03 and 0.13) respectively.

As noted previously, photoionization cross section calculations have been made recently on this complex ion using AUTOSTRUCTURE [4] within the Multi-Configuration-Breit-Pauli (MCBP) distorted-wave approximation for a wider range of energies and for higher charged states of the ion. Using this distorted wave approximation the authors find that the direct PI cross sections for these Se ions differ by 30% to 50% when compared to the available ALS experimental measurements. It was concluded from that study on Se ions [4] (by visual comparison) that best

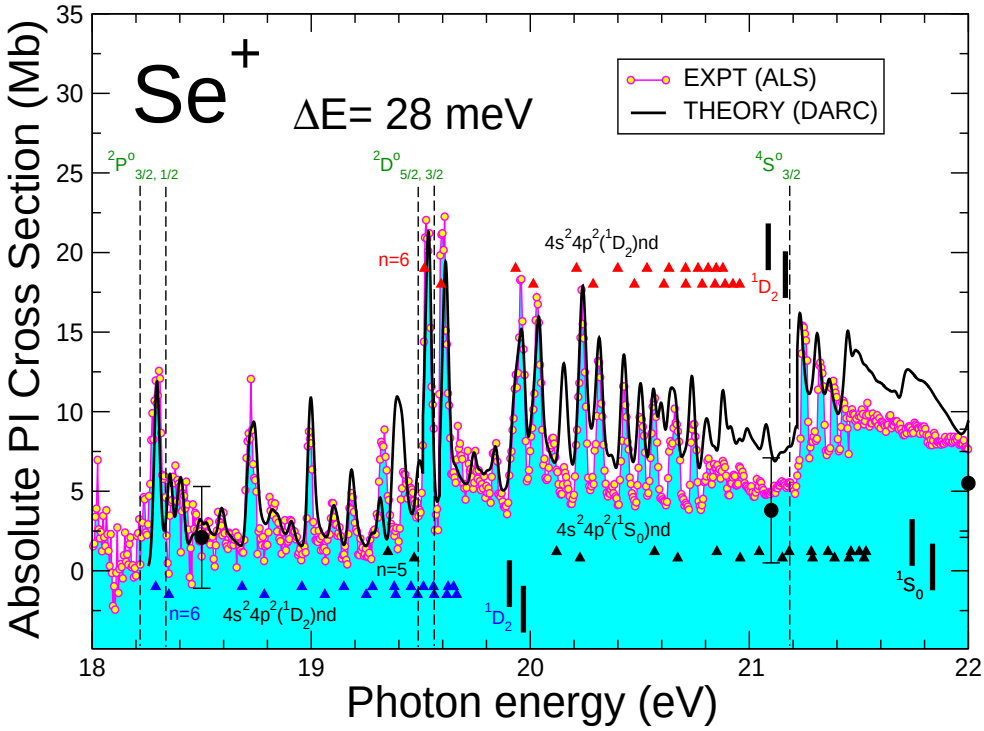


**Figure 4.** (Colour online) Comparison of ALS photoionization cross-section measurements from 18 eV to 21 eV taken at 28 meV (shaded area) with the 336-state close-coupling DARC calculations. The theoretical cross sections (solid black line) for each of the five initial states have been convoluted with a 28 meV FWHM gaussian and a weighting of the states (see text for details) to simulate the measurements. The absolute measurements (solid black circles) have been obtained with a larger energy step. The error bars give the total uncertainty of the experimental data. The various Rydberg series are indicated

agreement with experiment was obtained by weighting the contribution of the ground configuration states ($^4S^o_{3/2}$, $^2D^o_{3/2}$, $^2D^o_{5/2}$, $^2P^o_{1/2}$, $^2P^o_{3/2}$) by (0.53, 0.15, 0.05, 0.11, 0.16) respectively. Therefore a non statistical distribution of the PI cross sections in both theoretical approaches is seen to provide the best agreement with experiment.

Furthermore the Fano profile in the PI cross section near 23.0 eV is not reproduced by the AUTOSTRUCTURE calculations [4] (R matrix techniques are necessary to reproduce resonance interference effects), and the lack of this interference causes the discrepancy in the direct cross section in this energy region. The calculated and experimental $Se^+$ direct cross sections agree to within 30% to 50% over the range of experimental energies, except above 30 eV, where the experimental measurements are more uncertain since only a single absolute measurement was made above 27 eV

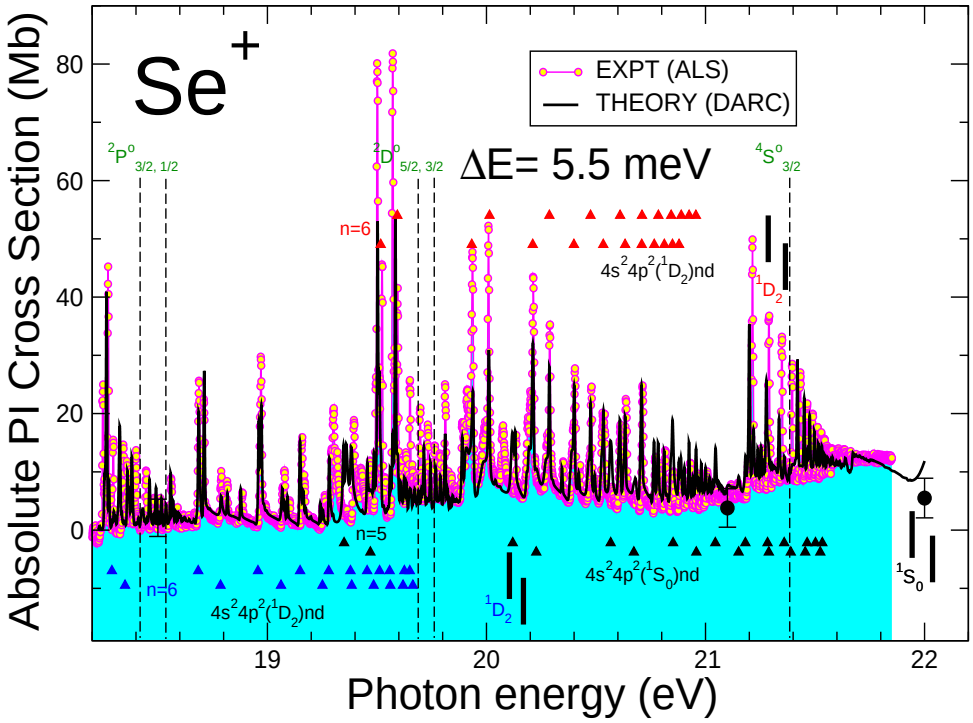


**Figure 5.** (Colour online) Comparison of ALS photoionization cross-section measurements from 18 eV to 21.8 eV taken at 5.5 meV (shaded area) with the 336-state close-coupling DARC calculations. The theoretical cross sections (solid black line) for each of the five initial states have been convoluted with a 5.5 meV FWHM gaussian and a weighting of the states (see text for details) to simulate the measurements. The absolute measurements (solid black circles) have been obtained with a larger energy step. The error bars give the total uncertainty of the experimental data. The various Rydberg series are indicated.

(compared to absolute measurements at lower energies, where independent estimates were performed 2 to 3 times for each energy). Therefore, they report uncertainties in the experiment of over 50 % in the high energy region. As R matrix techniques are necessary to reproduce resonance interference effects we have carried out these calculations in the present investigation.

In figure 4, the rich resonance structure observed in the experimental spectra is generally well represented in the metastable region by theory. This is still apparent when the theoretical work is compared with the experimental measurements taken at an even higher resolution [3]. Figure 5 shows the ALS experimental measurements taken at a higher resolution of 5.5 meV (from 18 eV to 21.8 eV) together with the theoretical results convoluted with a gaussian of the same FWHM to simulate the

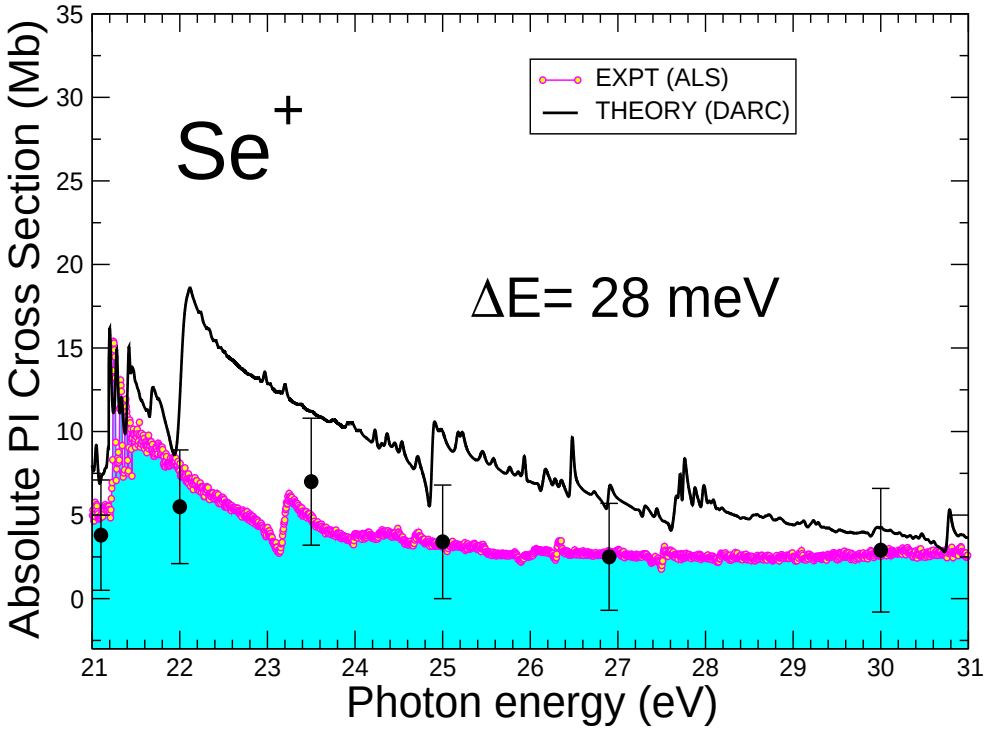


**Figure 6.** (Colour online) Comparison of ALS photoionization cross-section measurements from 21 eV to 31 eV taken at 28 meV (shaded area) with the 336-state close-coupling DARC calculations. The theoretical cross sections (solid black line) for each of the five initial states have been convoluted with a 28 meV FWHM gaussian and a weighting of the states (see text for details) to simulate the measurements. The absolute measurements (solid black circles) have been obtained with a larger energy step. The error bars give the total uncertainty of the experimental data.

experimental resolution and non-statistically weighted as before. Here again there is good agreement between the experimental and theoretical results.

In the energy region 21 eV to 31 eV, (figure 6) the theoretical results are larger than experiment. The solid line corresponds to the sum of the ground and metastable state fractions of the theoretical calculations. As indicated in the ALS experimental studies for $Se^+$ [1, 2], contamination from higher order radiation produced by the undulator beamline may be a possible cause for uncertainties. Previous experiments on $Xe^{3+}$ [42] estimated a lower fraction of 2 % at around 40 eV. The measurements on $Se^+$ [1, 2] are between these two photon energies and it was concluded in that work [1, 2] the maximum contamination is no greater than 4%. At lower photon energies, the contamination of higher order radiation is expected to be larger, but not by more

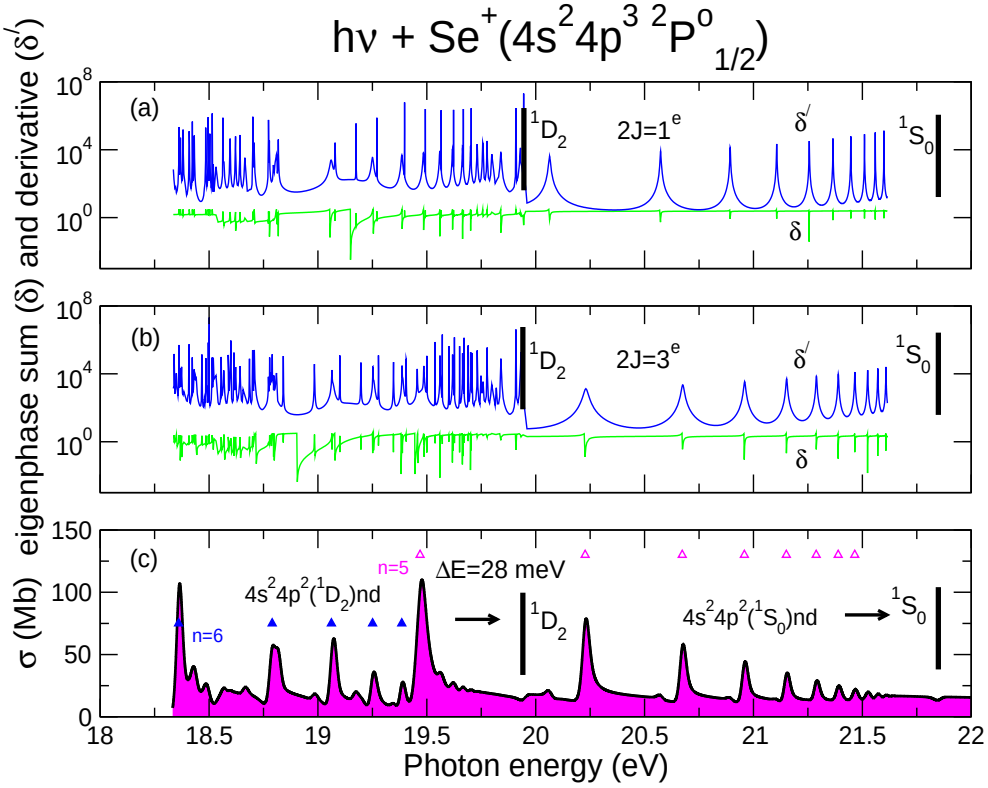


**Figure 7.** (Colour online) Eigenphase sum $\delta$ and its derivative $\delta'$ (for each $2J^{\pi}$ symmetry contributing to the PI cross section $\sigma$ for the $4s^24p^3\ {}^2P^o_{1/2}$ initial state) as a function of photon energy in the region below the $^1D_2$ and $^1S_0$ excited state thresholds of the residual $Se^{2+}$ ion for (a) $2J=1^e$ symmetry, (b) $2J=3^e$ symmetry and (c) PI cross section $\sigma$ for the $^2P^o_{1/2}$ metastable state convoluted with a gaussian of 28 meV FWHM (solid black line). The prominent Rydberg resonances series in the PI cross section have been identified (open and solid triangles) as members of two different Rydberg autoionizing series converging to the $^1D_2$ and $^1S_0$ excited states of the residual $Se^{2+}$ ion indicated by thick vertical lines.

than a factor of 2Ð3 compared to the contamination at 40 eV. It was concluded from the $Se^+$ ALS measurements [1, 2] that the experimental uncertainties on the absolute measurements made are estimated to be 30% including the possible contamination of the photon beam by higher order radiation.

Earlier studies on the photoionization spectrum of $O^+$ at the Advanced Light Source synchrotron radiation facility [43] were used to identify the resonance structure due to the metastable states [1, 2]. This is apparent when the spectra of $O^+$ and $Se^+$ are compared, the resemblance is remarkable but not totally unexpected. These respective ions have an $np^3$ configuration (n=2 for $O^+$ and n=4 for $Se^+$) in their

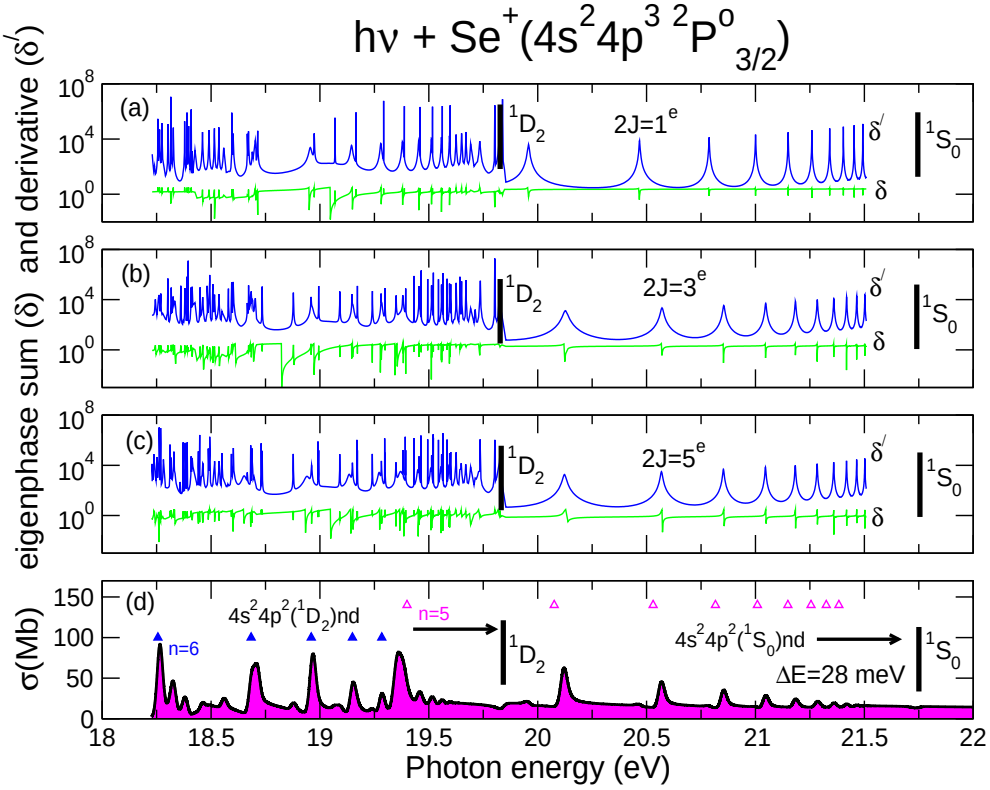


**Figure 8.** (Colour online) Eigenphase sum $\delta$ and its derivative $\delta'$ (for each $2J^{\pi}$ symmetry contributing to the PI cross section $\sigma$ for the $4s^24p^3\ ^2P^o_{3/2}$ initial state) as a function of photon energy in the region below the $^1D_2$ and $^1S_0$ excited state thresholds of the residual $Se^{2+}$ ion for (a) $2J=1^e$ symmetry, (b) $2J=3^e$ symmetry, (c) $2J=5^e$ symmetry and (d) PI cross section $\sigma$ for the $^2P^o_{3/2}$ metastable state convoluted with a gaussian of 28 meV FWHM (solid black line). The prominent Rydberg resonances series in the PI cross section have been identified (open and solid triangles) as members of two different Rydberg autoionizing series converging to the $^1D_2$ and $^1S_0$ excited states of residual $Se^{2+}$ ion indicated by thick vertical lines.

outermost shell giving rise in each case to the same term designation for the $^4S^o_{3/2}$ ground state and the $^2D^o_{3/2,5/2}$ and $^2P^o_{1/2,3/2}$ metastable states. In the case of $O^+$, the region of the spectrum covering the energy range from the $^2P^o_{1/2,3/2}$ threshold to the $^4S^o_{3/2}$ threshold consisted of very strong resonances due to $2p \rightarrow nd$ electron excitations of the metastable ions as well as weak resonances due to $2p \rightarrow ns$ transitions. Similarly, the $Se^+$ spectra, shows the corresponding $4p \rightarrow nd$ transitions but the $4p \rightarrow ns$ series appear to be too weak to be observed.

At energies below 21.2 eV there are prominent Rydberg resonance features resulting from photoionization of the initial metastable $Se^+$ states in the experimental

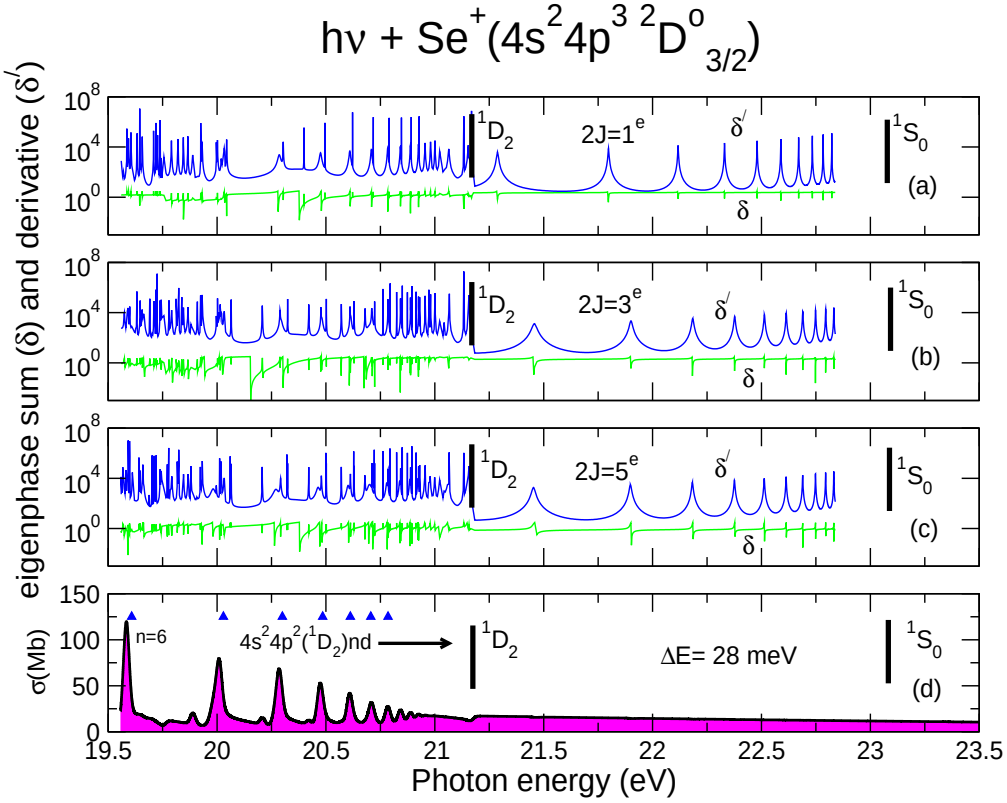


**Figure 9.** (Colour online) Eigenphase sum $\delta$ and its derivative $\delta'$ (for each $2J^{\pi}$ symmetry contributing to the PI cross section $\sigma$ for the $4s^24p^3\ ^2D^o_{3/2}$ initial state) as a function of photon energy in the region below the $^1D_2$ and $^1S_0$ excited state thresholds the residual $Se^{2+}$ ion for (a) $2J{=}1^e$ symmetry, (b) $2J{=}3^e$ symmetry, (c) $2J{=}5^e$ symmetry and (d) PI cross section $\sigma$ for the $^2D^o_{3/2}$ metastable state convoluted with a gaussian of 28 meV FWHM (solid black line). The prominent Rydberg resonances series in the PI cross section have been identified (solid triangles) as members of a Rydberg autoionizing series converging to the $^1D_2$ threshold of the residual $Se^{2+}$ ion. The weak resonance series converging to the $^1S_0$ threshold is not observed in the PI cross sections.

and theoretical cross sections, as is seen in figure 3. Multiple overlapping Rydberg resonance series in the spectra are also clearly visible converging to the $4s^24p^2\ ^1D_2$ and $4s^24p^2\ ^1S_0$ thresholds respectively of the residual $Se^{2+}$ ion. The presence of interloping resonances disrupt the regular Rydberg pattern of resonances, as can be seen in the spectra for the $^2P^o_{1/2}$ and $^2P^o_{3/2}$ metastable states, respectively figures 7 and 8.

To obtain the resonance parameters a theoretical analysis with a modification to the widely used eigenphase derivative (QB) technique (for $jj$ -coupling) that determines resonance parameters in electron collisions with atomic and molecular systems [39, 40, 41] was used. This technique exploits the properties of the R-matrix

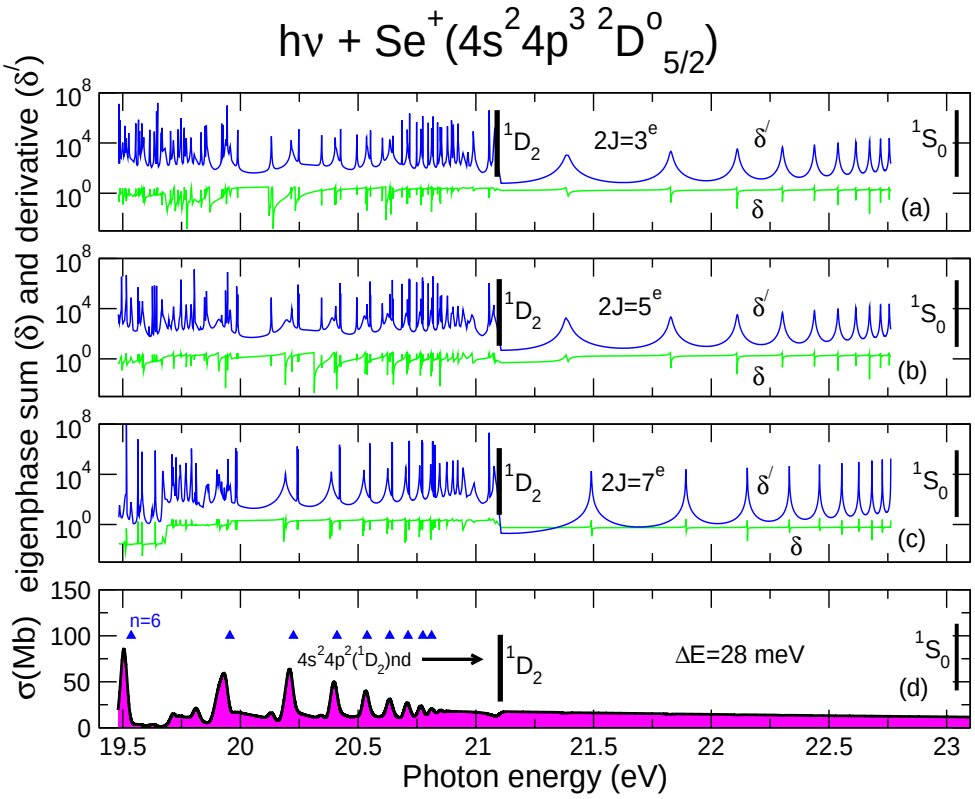


**Figure 10.** (Colour online) Eigenphase sum $\delta$ and its derivative $\delta'$ (for each $2J^{\pi}$ symmetry contributing to the PI cross section $\sigma$ for the $4s^24p^3\ ^2D^o_{5/2}$ initial state) as a function of photon energy in the region below the $^1D_2$ and $^1S_0$ excited state thresholds of the residual $Se^{2+}$ ion for (a) $2J=3^e$ symmetry, (b) $2J=5^e$ symmetry, (c) $2J=7^e$ symmetry and (d) PI cross section $\sigma$ for the $^2D^o_{5/2}$ metastable state convoluted with a gaussian of 28 meV FWHM (solid black line). The prominent Rydberg resonances series in the PI cross section have been identified (solid triangles) as members of a Rydberg autoionizing series converging to the $^1D_2$. The weak resonance series converging to the $^1S_0$ threshold is not observed in the PI cross sections.

in multi-channel scattering and is an excellent method for locating and determining the properties of narrow resonances. For this trans-iron element our theoretical results (obtained for the dominant resonance features in the photoionization spectra) are compared with the recent ALS measurements [1, 2]. From the ALS measurements [1, 2] it was shown that the $^2P^o_{1/2}$ and $^2P^o_{3/2}$ initial metastable states of the $Se^+$ ion both produce two dominant Rydberg resonance series. Our results for these resonances are illustrated in figure 7 and 8. The $4s^24p^2(^1D_2)$ nd series converging to the $^1D_2$ series limit is indicated with solid triangles and the $4s^24p^2(^1S_0)$ nd series converging to the $^1S_0$ limit by the open triangles. Furthermore, two additional autoionizing

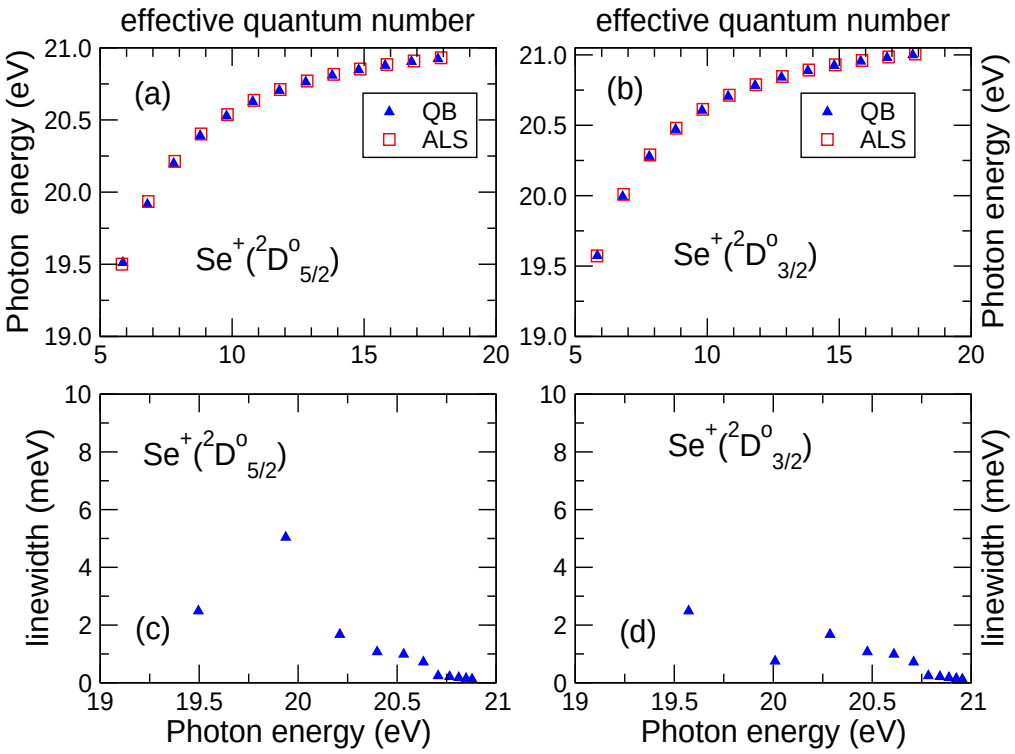


**Figure 11.** (Colour online) Effective quantum number $\nu$ = n - $\mu$ and the linewidth $\Gamma$ (meV) versus photon energy (eV) for the $4s^24p^2(^1D_2)$nd resonances lying below the $^1D_2$ threshold of the residual $Se^{2+}$ ion. Experimental data (open red squares, ALS [1, 2]) and theoretical estimates (solid blue triangles, QB); (a) effective quantum numbers ($\nu$) for the $4s^24p^2(^1D_2)$nd series originating from the initial $Se^+(^2D^o_{5/2})$ state; (b) effective quantum numbers ($\nu$) for the $4s^24p^2(^1D_2)$nd series originating from the initial $Se^+(^2D^o_{3/2})$ state; (c) $4s^24p^2(^1D_2)$nd, resonance linewidths ($\Gamma$) originating from the initial $Se^+(^2D^o_{5/2})$ state and (d) $4s^24p^2(^1D_2)$nd, resonance linewidths ($\Gamma$) originating from the initial $Se^+(^2D^o_{3/2})$ state.

Rydberg series were identified associated with the $^2D^o_{3/2}$ and $^2D^o_{5/2}$ metastable states, our theoretical results are shown by the solid triangles in figures 9 and 10.

The relationship between the principal quantum number n, the effective quantum number $\nu$ and the quantum defect $\mu$ for an ion of effective charge $\mathcal{Z}$ is given by $\nu$ = n $-$ $\mu$ where the resonance position $\epsilon_r$ can be determined from Rydberg's formula

$$\epsilon_r = \epsilon_\infty - \ \mathcal{Z}^2/\nu^2, \tag{2}$$

and $\epsilon_\infty$ is the resonance series limit [44]. Tables 2 – 5 lists the principal quantum number n, resonance energy $\epsilon_r$ and quantum defect $\mu$ of the first few members obtained

**Table 2.** Principal quantum number (n), resonance energies E (eV) and quantum defect ($\mu$) from experimental measurements of $Se^+$ [1, 2] compared with present theoretical estimates from the QB method. The Rydberg series originating from the $^2P^o_{3/2}$ metastable state of $Se^+$ due to 4p $\rightarrow$ nd transitions is tabulated. The uncertainties in the experimental energies are stated to be $\pm$0.010 eV or less. The series limits are taken from the NIST [38] tabulations and from Esteves and co-workers [1, 2].

| **Initial $Se^+$ state** $4s^24p^3$ ($^2P^o_{3/2}$) | | | **Initial $Se^+$ state** $4s^24p^3$ ($^2P^o_{3/2}$) | | |
|---|---|---|---|---|---|
| Rydberg Series $4s^24p^2(^1D_2)$ nd | | | Rydberg Series $4s^24p^2(^1D_2)$ nd | | |
| n | E (eV) | $\mu$ | n | E (eV) | $\mu$ |
| | [Theory] | | | [Experiment] | |
| 6 | 18.256 | 0.14 | 6 | 18.268 | 0.14 |
| 7 | 18.684 | 0.15 | 7 | 18.697 | 0.14 |
| 8 | 18.957 | 0.16 | 8 | 18.972 | 0.14 |
| 9 | 19.149 | 0.14 | 9 | 19.160 | 0.14 |
| 10 | 19.280 | 0.16 | 10 | 19.296 | 0.12 |
| 11 | 19.379 | 0.15 | 11 | 19.395 | 0.10 |
| 12 | 19.455 | 0.14 | - | - | - |
| . | . | - | . | . | - |
| $\infty$ | 19.842$^\dagger$ | | $\infty$ | 19.853 $\pm$ 0.05$^\ddagger$ | |

$^\dagger$NIST tabulations [38]
$^\ddagger$Esteves PhD thesis [1]

from our work for each of the prominent Rydberg series originating from the $^2P^o_{3/2}$ and $^2P^o_{1/2}$ metastable states. The experimental results of Esteves and co-workers [1, 2] are included in Tables 2– 5 for comparison purposes where it is seen our theoretical work is in satisfactory agreement with experiment for the resonance energies and quantum defects. Measurements taken at the Advanced Light Source synchrotron radiation facility indicated the presence of several prominent $4s^24p^2(^1D_2)$ nd resonances in this energy range originating from the $^2D^o_{5/2}$ and $^2D^o_{3/2}$ initial metastable states. Tables 6 and 7 present results for the $4s^24p^2(^1D_2)$ nd dominant resonance series observed in the PI cross sections originating from the $^2D^o_{3/2}$ and $^2D^o_{5/2}$ metastable states respectively. Here again our theoretical work show satisfactory agreement with experiment for the resonance energies and quantum defects.

Finally, from figure 11, theoretical estimates indicate many of the linewidths ($\Gamma$, determined from the QB method) for the $4s^24p^2(^1D_2)$ nd series are less than a few meV, making their experimental determination challenging. Overall, given the complexity of this trans-iron element and the wealth of resonance structure in the corresponding PI cross sections, the agreement between theory and experiment is very satisfactory.

**Table 3.** Principal quantum number (n), resonance energies E (eV) and quantum defect ($\mu$) from experimental measurements of $Se^+$ [1, 2] compared with present theoretical estimates from the QB method. The Rydberg series originating from the $^2P^o_{3/2}$ metastable state of $Se^+$ due to 4p $\rightarrow$ nd transitions is tabulated. The uncertainties of the experimental energies are stated to be $\pm$0.010 eV. The series limits are taken from the NIST [38] tabulations and from Esteves and co-workers [1, 2].

| **Initial $Se^+$ state** $4s^24p^3$ ($^2P^o_{3/2}$) | | | **Initial $Se^+$ state** $4s^24p^3$ ($^2P^o_{3/2}$) | | |
|---|---|---|---|---|---|
| Rydberg Series $4s^24p^2(^1S_0)$ nd | | | Rydberg Series $4s^24p^2(^1S_0)$ nd | | |
| n | E (eV) | $\mu$ | n | E (eV) | $\mu$ |
| | [Theory] | | | [Experiment] | |
| 5 | 19.350 | 0.24 | 5 | 19.301 | 0.22 |
| 6 | 20.118 | 0.23 | 6 | 20.074 | 0.22 |
| 7 | 20.556 | 0.22 | 7 | 20.530 | 0.19 |
| 8 | 20.851 | 0,22 | 8 | 20.815 | 0.17 |
| 9 | 21.044 | 0.22 | 9 | 21.008 | 0.15 |
| 10 | 21.181 | 0.22 | 10 | 21.149 | 0.10 |
| 11 | 21.283 | 0.22 | - | - | - |
| 12 | 21.359 | 0.22 | - | - | - |
| . | . | – | . | . | - |
| $\infty$ | 21.751$^\dagger$ | | $\infty$ | 21.703$\pm$ 0.05 $^\dagger$ | |

$^\dagger$NIST tabulations [38]
$^\ddagger$Esteves PhD thesis [1]

## 4. Conclusions

State-of-the-art theoretical methods were used to investigate the photoionization of $Se^+$ ions in the energy region of the ground-state ionization threshold (18 eV – 31 eV). Given the complexity of this trans-iron element, overall, satisfactory agreement is found between theoretical and experimental results both on the photon-energy scale and on the absolute PI cross-section scale. The photoionization cross section exhibits a wealth of resonances. Prominent members of the Rydberg series are analyzed and compared with experiment. Resonance positions and quantum defects for the $4s^24p^2(^1D_2)$nd and $4s^24p^2(^1S_0)$nd series converging to their respective series limits are presented. The metastable state content of the $Se^+$ ion beam has been determined along with prominent autoionizing Rydberg resonances series seen in the experimental PI cross sections. A clear pattern of Rydberg resonance series is seen in the spectra of the photoionization cross sections disrupted by interloping resonances (see figures 4 and 5).

We point out that the strength of the present study is in the convergence between two different state-of-the-art theoretical methods and the comparison with available experimental data. Since no beam diagnostics were carried out in the experiments

**Table 4.** Principal quantum number (n), resonance energies E (eV) and quantum defect ($\mu$) from experimental measurements of $Se^+$ [1, 2] compared with present theoretical estimates from the QB method. The Rydberg series originating from the $^2P^o_{1/2}$ metastable state of $Se^+$ due to 4p $\rightarrow$ nd transitions is tabulated. The uncertainties of the experimental energies are stated to be $\pm$0.010 eV. The series limits are taken from the NIST [38] tabulations and from Esteves and co-workers [1, 2].

| **Initial $Se^+$ state** $4s^24p^3$ ($^2P^o_{1/2}$) | | | **Initial $Se^+$ state** $4s^24p^3$ ($^2P^o_{1/2}$) | | |
|---|---|---|---|---|---|
| Rydberg Series $4s^24p^2(^1D_2)$ nd | | | Rydberg Series $4s^24p^2(^1D_2)$ nd | | |
| n | E (eV) | $\mu$ | n | E (eV) | $\mu$ |
| | [Theory] | | | [Experiment] | |
| 6 | 18.345 | 0.17 | 6 | 18.354 | 0.17 |
| 7 | 18.786 | 0.16 | 7 | 18.788 | 0.17 |
| 8 | 19.062 | 0.16 | 8 | 19.070 | 0.16 |
| 9 | 19.251 | 0.16 | 9 | 19.262 | 0.14 |
| 10 | 19.385 | 0.16 | 10 | 19.298 | 0.12 |
| 11 | 19.485 | 0.16 | - | - | - |
| 12 | 19.561 | 0.15 | - | - | - |
| . | . | - | - | . | - |
| $\infty$ | 19.842$^\dagger$ | | | 19.853 $\pm$ 0.05$^\ddagger$ | |

$^\dagger$NIST tabulations [38]
$^\ddagger$Esteves PhD thesis [1]

[1, 2] it is left to theory to infer the appropriate fractions. Such detailed comparisons, between theory and experiment, strengthens the validity of our results for use in astrophysical applications.

The photoionization cross-sections from the present study are suitable to be included into state-of-the-art photoionization modelling codes Cloudy and XSTAR [19, 20] that are used to numerically simulate the thermal and ionization structure of ionized astrophysical nebulae. In combination with our determinations of the photoionization properties of other low-charge Se ions (to be addressed in subsequent publications), this will enable the abundance of Se to be accurately determined in astrophysical nebulae. Such information bears implications for the sites of origin and chemical evolution of Se and other trans-iron elements in the Universe, as well as for studies of the interior structure and nucleosynthesis of giant stars. These recent modifications to the Dirac-Atomic-R-matrix-Codes (DARC) have now made it feasible to systematically study other heavy complex systems of prime interest to astrophysics.

## Acknowledgments

C P Ballance was supported by US Department of Energy (DoE) grants through Auburn University. B M McLaughlin acknowledges support by the US National

**Table 5.** Principal quantum number (n), resonance energies E (eV) and quantum defect ($\mu$) from experimental measurements of $Se^+$ [1, 2] compared with present theoretical estimates from the QB method. The Rydberg series originating from the $^2P^o_{1/2}$ metastable state of $Se^+$ due to 4p $\rightarrow$ nd transitions is tabulated. The uncertainties in the experimental energies are stated to be $\pm$0.010 eV. The series limits are taken from the NIST [38] tabulations and from Esteves and co-workers [1, 2].

| **Initial $Se^+$ state** $4s^24p^3$ ($^2P^o_{1/2}$) | | | **Initial $Se^+$ state** $4s^24p^3$ ($^2P^o_{1/2}$) | | |
|---|---|---|---|---|---|
| Rydberg Series $4s^24p^2(^1S_0)$ nd | | | Rydberg Series $4s^24p^2(^1S_0)$ nd | | |
| n | E (eV) | $\mu$ | n | E (eV) | $\mu$ |
| | [Theory] | | | [Experiment]‡ | |
| 5 | 19.469 | 0.23 | 5 | 19.468 | 0.17 |
| 6 | 20.227 | 0.22 | 6 | 20.202 | 0.17 |
| 7 | 20.673 | 0.22 | 7 | 20.637 | 0.17 |
| 8 | 20.958 | 0.22 | 8 | 20.922 | 0.15 |
| 9 | 21.151 | 0.22 | 9 | 21.116 | 0.11 |
| 10 | 21.288 | 0.22 | 10 | 21.238 | 0.20 |
| 11 | 21.389 | 0.22 | - | - | - |
| 12 | 21.465 | 0.22 | - | - | - |
| . | . | - | . | . | - |
| $\infty$ | 21.857† | | $\infty$ | 21.805 $\pm$ 0.05† | |

†NIST tabulations [38]
‡Esteves PhD thesis [1]

Science Foundation through a grant to ITAMP at the Harvard-Smithsonian Center for Astrophysics. We thank David A Esteves for providing us with the ALS experimental data and a copy of his thesis. The computational work was carried out at the National Energy Research Scientific Computing Center in Oakland, CA, USA and on the Teragrid at the National Institute for Computational Sciences (NICS) in Knoxville, TN, USA.

**Table 6.** Principal quantum number (n), resonance energies E (eV) and quantum defect ($\mu$) from experimental measurements of $Se^+$ [1, 2] compared with present theoretical estimates from the QB method. The Rydberg series originating from the $^2D^o_{5/2}$ metastable state of $Se^+$ due to 4p $\rightarrow$ nd transitions is tabulated. The uncertainties in the experimental energies are stated to be $\pm$0.010 eV. The series limits are taken from the NIST [38] tabulations and from Esteves and co-workers [1, 2].

| **Initial $Se^+$ state** $4s^24p^3$ ($^2D^o_{5/2}$) | | | **Initial $Se^+$ state** $4s^24p^3$ ($^2D^o_{5/2}$) | | |
|---|---|---|---|---|---|
| Rydberg Series $4s^24p^2(^1D_2)$ nd | | | Rydberg Series $4s^24p^2(^1D_2)$ nd | | |
| n | E (eV) | $\mu$ | n | E (eV) | $\mu$ |
| | [Theory] | | | [Experiment] | |
| 6 | 19.496 | 0.17 | 6 | 19.499 | 0.17 |
| 7 | 19.938 | 0.15 | 7 | 19.933 | 0.17 |
| 8 | 20.211 | 0.16 | 8 | 20.212 | 0.17 |
| 9 | 20.399 | 0.16 | 9 | 20.402 | 0.16 |
| 10 | 20.533 | 0.16 | 10 | 20.537 | 0.17 |
| 11 | 20.633 | 0.16 | 11 | 20.637 | 0.16 |
| 12 | 20.707 | 0.16 | 12 | 20.712 | 0.16 |
| . | . | - | . | . | - |
| $\infty$ | 21.095[†] | | $\infty$ | 21.100$\pm$ 0.01[‡] | |

[†]NIST tabulations [38]
[‡]Esteves PhD thesis [1]

**Table 7.** Principal quantum number (n), resonance energies E (eV) and quantum defect ($\mu$) from experimental measurements of $Se^+$ [1, 2] compared with present theoretical estimates from the QB method. The Rydberg series originating from the $^2D^o_{3/2}$ metastable state of $Se^+$ due to 4p $\rightarrow$ nd transitions is tabulated. The uncertainties in the experimental energies are stated to be $\pm$0.010 eV. The series limits are taken from the NIST [38] tabulations and the work of Esteves and co-workers [1, 2].

| **Initial $Se^+$ state** $4s^24p^3$ ($^2D^o_{3/2}$) | | | **Initial $Se^+$ state** $4s^24p^3$ ($^2D^o_{3/2}$) | | |
|---|---|---|---|---|---|
| Rydberg Series $4s^24p^2(^1D_2)$ nd | | | Rydberg Series $4s^24p^2(^1D_2)$ nd | | |
| n | E (eV) | $\mu$ | n | E (eV) | $\mu$ |
| | [Theory] | | | [Experiment] | |
| 6 | 19.573 | 0.17 | 6 | 19.572 | 0.18 |
| 7 | 20.009 | 0.16 | 7 | 20.009 | 0.17 |
| 8 | 20.287 | 0.16 | 8 | 20.289 | 0.17 |
| 9 | 20.476 | 0.16 | 9 | 20.479 | 0.16 |
| 10 | 20.610 | 0.16 | 10 | 20.613 | 0.17 |
| 11 | 20.710 | 0.16 | 11 | 20.713 | 0.16 |
| 12 | 20.784 | 0.16 | 12 | 20.788 | 0.16 |
| . | . | - | . | . | - |
| $\infty$ | 21.172[†] | | $\infty$ | 21.176 $\pm$ 0.025[‡] | |

[†]NIST tabulations [38]
[‡]Esteves PhD thesis [1]

[1] Esteves D A 2010 *Photoionization of Se Ions for the Determination of Elemental Abundances in Astrophysical Nebulae,* Thesis (Ph. D.); Publication Number: AAI3404727, University of Reno, Nevada, USA URL `http://proquest.umi.com/pqdlink?did=2112569361&Fmt=7&clientId=79356&RQT=309&VName=PQD`

[2] Sterling N C *et al* 2011 *J. Phys. B: At. Mol. Opt. Phys.* **44** 025701

[3] Esteves D A *et al* 2011 *Phys. Rev. A* **84** 013406

[4] Sterling N C and Witthoeft M 2011 *Astron. Astrophys.* **529** A147

[5] Sterling N C, Dinerstein H L, Hwang S, Redfield S, Aguilar A, Witthoeft M C, Esteves D, Kilcoyne A L D, Bautista M, Phaneuf R A, Bilodeau R, Ballance C P, McLaughlin B M and Norrington P H 2009 *Pub. Astron. Soc. Aust. (PASA)* **26** 339

[6] Sterling N C *et al* 2011 *Can. J. Phys.* **89** 379

[7] Sterling N C, Dinerstein H L and Kallman T R 2007 *Astrophys. J. Suppl. Ser.* **169** 37

[8] Sharpee B, Zhang Y, Williams R, Pellegrini E, Cavagnolo K, Baldwin J A, Phillips M and Liu X W 2007 *Astrophys. J.* **659** 1265

[9] Sterling N C and Dinerstein H L 2008 *Astrophys. J. Suppl. Ser.* **174** 157

[10] Langanke K and Wiescher M 2001 *Rep. Prog. Phys.* **64** 1657

[11] Smith V V and Lambert D L 1990 *Astrophys. J. Suppl. Ser.* **72** 387

[12] Cardelli J A, Federman S R, Lambert D L and Theodosiou C E 1993 *Astrophys. J* **416** L41

[13] Wallerstein, G *et al* 1997 *Rev. Modern Phys.* **69** 995

[14] Busso M, Gallino R and Wasserburg G J 1999 *Ann. Rev. Astron. Astrophys.* **37** 239

[15] Travaglio C, Gallino R, Arnone E, Cowan J J, Jordan F and Sneden C 2004 *Astrophys. J* **601** 864

[16] Herwig F 2005 *Ann. Rev. Astron. Astrophys.* **43** 435

[17] Cowan J J and Sneden C 2006 *Nature* **440** 1151

[18] Straniero O, Gallino R and Cristallo S 2006 *Nucl. Phys. A* **777** 311

[19] Ferland G J, Korista K T, Verner D A, Ferguson J W, Kingdon J B and Verner E M 1998 *PASP* **110** 761

[20] Kallman T and Bautista M 2001 *Astrophys. J. Suppl. Ser.* **133** 221

[21] Lu M, Gharaibeh M F, AlnaÕwashi G, Phaneuf R A, Kilcoyne A L D, Levenson E, Schlachter A S, Müller A, Schippers S, Jacobi J, Scully S W J and Cisneros C 2006 *Phys. Rev. A* **74** 012703

[22] Lu M, AlnaÕwashi G, Habibi M, Gharaibeh M F, Phaneuf R A, Kilcoyne A L D, Levenson E, Schlachter A S, and Cisneros C and Hinojosa G 2006 *Phys. Rev. A* **74** 062701

[23] Bizau J M *et al* 2011 *J. Phys. B: At. Mol. Opt. Phys.* **44** 055205

[24] Bizau J M, Blancard C, Cubaynes D, Folkmann F, Champeaux J P, Lemaire J L and Wuilleumier F J 2006 *Phys. Rev. A* **73** 022718

[25] Grant I P 2007 *Quantum Theory of Atoms and Molecules: Theory and Computation* (New York, USA: Springer)

[26] Ballance C P and Griffin D C 2004 *J. Phys. B: At. Mol. Opt. Phys.* **37** 2943

[27] Hummer D G, Berrington K A, Eissner W, Pradhan A K, Saraph H E and Tully J A 1993 *Astron. Astrophys.* **279** 298

[28] Ballance C P, Griffin D C and B M McLaughlin 2007 *J. Phys. B: At. Mol. Opt. Phys.* **40** F327

[29] Ballance C P and Griffin D C 2008 *J. Phys. B: At. Mol. Opt. Phys.* **41** 195205

[30] Ballance C P and Griffin D C 2006 *J. Phys. B: At. Mol. Opt. Phys.* **39** 3617

[31] Norrington P H and Grant I P 1987 *J. Phys. B: At. Mol. Opt. Phys.* **20** 4869

[32] Wijesundera W P, Parpia F A, Grant I P and Norrington P H 1991 *J. Phys. B: At. Mol. Opt. Phys.* **24** 1803

[33] Norrington P H 1991 *J. Phys. B: At. Mol. Opt. Phys.* **24** 1803

[34] Norrington P H DARC codes URL, `http://web.am.qub.ac.uk/DARC`

[35] McLaughlin B M and Ballance C P 2012 *J. Phys. B: At. Mol. Opt. Phys.* in press

[36] Dyall K G, Grant I P, Johnson C T and Plummer E P 1989 *Comput. Phys. Commun.* **55** 425

[37] Parpia F, Froese Fischer C and Grant I P 2006 *Comput. Phys. Commun.* **94** 249

[38] Ralchenko Y, Kramida A E, Reader J, and NIST ASD Team (2011), NIST Atomic Spectra Database (version 4.0.1), National Institute of Standards and Technology, Gaithersburg, MD, USA, URL `http://physics.nist.gov/asd3`

[39] Quigley L and Berrington K A 1996 *J. Phys. B: At. Mol. Phys.* **29** 4529

[40] Quigley L, Berrington K A and Pelan J 1998 *Comput. Phys. Commun.* **114** 225

[41] Ballance C P, Berrington K A and McLaughlin B M 1999 *Phys. Rev. A* **60** R4217

[42] Emmons E D, Aguilar A, Gharaibeh M F, Scully S W J, Phaneuf R A, Kilcoyne A L D, Schlachter A S, Álvarez I, Cisneros C, and Hinojosa G 2005 *Phys. Rev. A* **71** 042704

[43] Aguilar A, Covington A M, Hinojosa G, Phaneuf R A, Álvarez I, Cisneros C, Bozek J D,

Dominguez, I, Sant'Anna M M, Schlachter A S, Nahar S N, McLaughlin B M 2003 *Astrophys. J. Suppl. Ser.* **146** 467
[44] Seaton M J 1983 *Rep. Prog. Phys* **46** 167–257